

## THE DISTANCE TO THE LARGE MAGELLANIC CLOUD FROM ECLIPSING BINARIES II. HV 982<sup>1</sup>

E.L. FITZPATRICK, I. RIBAS<sup>2</sup>, E.F. GUINAN<sup>2</sup>, L.E. DEWARP<sup>2</sup>, F.P. MALONEY

Department of Astronomy & Astrophysics, Villanova University, Villanova, PA 19085

D. MASSA

Raytheon ITSS

*To appear in the Astrophysical Journal, March 2001*

### ABSTRACT

We have determined the distance to a second eclipsing binary system (EB) in the Large Magellanic Cloud, HV 982 ( $\sim$ B1 IV-V +  $\sim$ B1 IV-V). The measurement of the distance — among other properties of the system — is based on optical photometry and spectroscopy and space-based UV/optical spectrophotometry. The analysis combines the “classical” EB study of light and radial velocity curves, which yield the stellar masses and radii, with a new analysis of the observed energy distribution, which yields the effective temperature, metallicity, and reddening of the system plus the distance “attenuation factor”, essentially  $(\text{radius}/\text{distance})^2$ . Combining the results gives the distance to the system, which is  $45.6 \pm 2.1$  kpc.

This distance determination is extremely robust. It consists of a detailed study of well-understood objects (B stars) in a well-understood evolutionary phase (core H burning). The results are entirely consistent with — but do not depend on — stellar evolution calculations. There are no “zeropoint” uncertainties as, for example, with the use of Cepheid variables. Neither is the result subject to sampling biases, as may affect techniques which utilize whole stellar populations, such as red giant stars. Moreover, the analysis is insensitive to stellar metallicity (although the metallicity of the stars is explicitly determined) and the effects of interstellar extinction are determined for each object studied.

After correcting for the location of HV 982, we find a distance to the optical center of the LMC’s bar of  $d_{\text{LMC}} = 45.9 \pm 2.1$  kpc or  $(V_0 - M_V)_{\text{LMC}} = 18.31$  mag. This result is entirely consistent with our earlier result for the EB HV 2274, which yielded  $(V_0 - M_V)_{\text{LMC}} = 18.30 \pm 0.07$  mag. These results argue strongly in favor of the “short” LMC distance scale.

*Subject headings:* Binaries: Eclipsing - Stars: Distances - Stars: Fundamental Parameters - Stars: Individual (HV 982) - Galaxies: Magellanic Clouds - Cosmology: Distance Scale

### 1. INTRODUCTION

The distance to the Large Magellanic Cloud (LMC) is a key factor in determining the size scale of the universe. Indeed, the uncertainty in the length of this “cosmic meter stick” is responsible for much of the current uncertainty in the value of the Hubble constant, as noted by Mould et al. (2000). As important as it is to astrophysics, the LMC distance is equally controversial. Existing determinations span a wide range (see Fig. 1 of Mould et al.) and are often grouped into the “long” distance scale results ( $d > 50$  kpc and  $(V_0 - M_V) \simeq 18.7$  mag) and the “short” distance scale results ( $d < 50$  kpc and  $(V_0 - M_V) \simeq 18.3$  mag). In some cases, the same technique (e.g., Cepheids) can support both the long and short scales, depending on the assumptions and details of the analysis. Reviews of LMC distance determinations can be found in Westerlund (1997) and Cole (1998), and numerous new papers have appeared in the last 2 years indicating the high activity level and interest in the field.

Recently, we showed that well-detached main sequence B-type eclipsing binary (EB) systems are virtually ideal standard candles and have the potential to resolve the LMC distance controversy (Guinan et al. 1998; hereafter Paper I). The advantages of using EBs are manyfold. First, a precise distance can be de-

termined for each individual system — and there are many systems. This is in contrast to techniques that utilize, for example, Cepheids or red giant stars, where the entire observed population is used to derive a single distance estimate. It also contrasts with techniques that utilize SN1987A, which have the potential to yield a precise distance but for which there is only one object to study. The EBs can provide not only the mean LMC distance, but also can be used to probe the structure of the LMC. Second, the analysis involves well-understood objects in a well-understood phase of stellar evolution (core hydrogen burning) and the results for each object can be verified independently by — but do not depend on — stellar evolution theory. Third, the analysis is robust and not subject to any zeropoint uncertainties, nor are there any adjustable parameters. For example, the results are extremely insensitive to stellar metallicity, although the metallicity of the individual EBs is explicitly determined and incorporated in the analysis. Likewise, the determination of interstellar extinction is an integral part of the analysis of each object.

The study of the EB system HV 2274 in Paper I yielded a distance of  $46.8 \pm 1.6$  kpc and stellar properties completely consistent with stellar evolution theory (Ribas et al. 2000a). Correcting for the position of HV 2274 relative to the LMC center yielded a LMC distance of  $45.7 \pm 1.6$  kpc corresponding

<sup>1</sup>Based on observations with the NASA/ESA Hubble Space Telescope, obtained at the Space Telescope Science Institute, which is operated by the Association of Universities for Research in Astronomy, Inc. under NASA contract No. NAS5-26555.

<sup>2</sup>Visiting Astronomer, Cerro Tololo Inter-American Observatory, National Optical Astronomy Observatories, which is operated by the Association of Universities for Research in Astronomy, Inc. (AURA) under cooperative agreement with the National Science Foundation.

to  $(V_0 - M_V) = 18.30 \pm 0.07$  mag. This result argues strongly in favor of the “short distance” to the LMC, but measurement of a single system cannot be considered definitive. Studies of other systems located in different parts of the LMC, with different stellar properties, and different interstellar properties (i.e., redenings) are clearly desired.

In this paper, we apply our analysis to a second LMC EB system, HV 982, and derive the stellar properties and its distance. This EB, with  $V \simeq 14.6$ , consists of two mildly evolved main sequence B stars each corresponding to spectral class  $\sim$ B1 IV–V. In §2, we describe the data included in this study. In §3, the analysis — which incorporates the light curve, radial velocity curve, and spectral energy distribution of the system — is discussed. The general properties of the system are described in §4 and their consistency with stellar evolution theory examined. Finally, the distance to HV 982 and the implied distance to the LMC is derived in §5, and the main conclusions are outlined in §6.

## 2. THE DATA

Three distinct datasets are required to carry out our analyses of the LMC EB systems: precise differential photometry (yielding light curves), high-resolution spectroscopy (yielding radial velocity curves) and multiwavelength spectrophotometry (yielding temperature and reddening information). Each of these three are described briefly below.

### 2.1. Optical Photometry

CCD differential photometric observations of HV 982 were reported by Pritchard et al. (1998; hereafter P98). These data were obtained between 1992 and 1995 with a 1-m telescope at Mt. John University Observatory (New Zealand). The resultant light curves in the Strömgren  $u$ , Johnson  $V$  and Cousins  $I$  passbands have very good phase coverage, with 132, 565, and 205 measurements, respectively. More sparsely-covered light curves were obtained in the Strömgren  $vby$  passbands, with 48, 45, and 44 measurements for  $v$ ,  $b$ , and  $y$ , respectively. The precision of the individual differential photometric measurements is  $0.010 - 0.015$  mag.

### 2.2. Optical Spectroscopy

Radial velocity curves for HV 982 and a number of other LMC EBs were derived from optical echelle spectra obtained by us in January 2000 with the Blanco 4-m telescope at Cerro Tololo Inter-American Observatory in Chile. The seeing conditions during the 6-night observing run ranged between 0.9 and 1.8 arcsec. We secured eight spectra of HV 982 — near orbital quadratures — covering the wavelength range 3600–5500 Å, with a resolution of  $\sim 0.07$  Å pix $^{-1}$  ( $4.7$  km s $^{-1}$  pix $^{-1}$ ), and a S/N of  $\sim 30:1$ . The exposure time per spectrum was 1800 sec, sufficiently short to avoid significant radial velocity shifts during the integrations. All the HV 982 observations were bracketed with ThAr comparison spectra for proper wavelength calibration. The raw images were reduced using standard NOAO/IRAF tasks (including bias subtraction, flat field correction, sky-background subtraction, cosmic ray removal, extraction of the orders, dispersion correction, and merging and continuum normalization). Spectra of radial velocity standard stars were acquired and reduced with the same procedure.

Visual inspection of the HV 982 spectra revealed prominent H Balmer lines and conspicuous lines of He I (4009, 4026, 4144, 4388, 4471 and 4922 Å). Various features due to ionized

C, Si, and O are also expected, but with strengths comparable to the noise level in the individual spectra. A section of one of the spectra, centered near the strong He I 4388 and 4471 Å lines, is shown in Figure 1. This spectrum was obtained at orbital phase 0.7252 and illustrates the clean velocity separation of the two components of the binary.

To fully exploit the velocity information in the data, we employed cross-correlation techniques for these measurements, utilizing the NOAO/IRAF routine FXCOR and restricting our attention to the 4000–5000 Å wavelength region. Data at higher and lower wavelengths were either badly contaminated with H Balmer lines or had very poor S/N, or both. The broad H Balmer lines are generally not suitable for radial velocity work because of blending effects, which lead to systematic underestimation of radial velocity amplitudes (see, e.g., Andersen 1975). In the 4000–5000 Å range, the H  $\beta$ , H  $\gamma$  and H  $\delta$  lines were masked by setting the normalized flux to unity in a window around their central wavelength. We used a very high S/N ( $\sim 250$ ) spectrum of HR 1443 ( $\delta$  Cae, B2 IV–V,  $v\sin i = 36$  km s $^{-1}$ ) as the velocity template. The template spectrum was convolved with a rotational broadening function to reproduce the line-width of the HV 982 components ( $v\sin i \simeq 100$  km s $^{-1}$ ). (Note that results derived without rotationally broadening the template spectrum are essentially identical.) Two cross-correlation function peaks (one per stellar component) were perfectly visible for all the object spectra, and in most cases were completely unblended, as might be anticipated from Figure 1. Gaussian fits to the peaks yielded the final radial velocities. An example of the cross-correlation function is shown in Figure 2 for the spectrum acquired at phase 0.7252.

The heliocentric radial velocities derived from all the CTIO spectra using the procedures outlined above are listed in Table 1 (“RV<sub>P</sub>” and “RV<sub>S</sub>”), along with their associated measurement errors, the date of observation, and the corresponding phase.

## 2.3. UV/Optical Spectrophotometry

We obtained spectrophotometric observations of HV 982 in the UV and optical wavelength regions with the Faint Object Spectrograph (FOS) aboard the *Hubble Space Telescope* during two observing sessions (12 November 1996 and 31 January 1997). Data were obtained in four wavelength regions, using the G130H, G190H, G270H, and G400H observing modes of the FOS. The spectral resolution of these data is about 1300 ( $\lambda/\Delta\lambda$ ). The data were processed and calibrated using the standard pipeline processing software for the FOS, and the final merged spectrum covers the range 1150 Å to 4820 Å. The observations of HV 982 were made at orbital phases outside of the eclipses, when both stars were completely unobscured.

## 3. THE ANALYSIS

Our study of HV 982 depends on three separate but interdependent analyses. These involve the light curve, the radial velocity curve, and the observed spectral energy distribution. The combined results provide essentially a complete description of the gross physical properties of the HV 982 system and a precise measurement of its distance. Each of the three analyses is described below.

### 3.1. The Light Curve

P98 ran simultaneous solutions for the 6 light curves described above in §2.1 using an improved version of the Wilson-Devinney program (Wilson & Devinney 1971; here-

after WD) that includes an atmosphere model routine developed by Milone et al. (1992) for the computation of the stellar radiative parameters. The WD program was run in an iterative mode in order to explore the full-extent of parameter space and also to make a realistic estimation of the errors. Furthermore, the authors considered different mass ratios ranging between 0.9 and 1.1 (since no spectroscopic observations were available at that time) and found the light curve solution to be completely insensitive to changes within this range.

As often occurs for eclipsing binary stars in eccentric orbits, several parameter sets — four in this case — were found to yield equally good fits to the observed light curves. The main distinction among the possible solutions is that P98's Cases 1 and 2 predict the primary star to be somewhat smaller and cooler than the secondary ( $L_S/L_P \simeq 1.1$ ), while Cases 3 and 4 yield a bigger and hotter primary ( $L_S/L_P \simeq 0.9$ ). This degeneracy can be broken only by considering some external source of information, e.g., a spectroscopically-determined luminosity ratio. Without such information, P98 were unable to favor any of their four cases.

For nearly-identical stars, the ratio of absorption line equivalent widths is related to the ratio of the continuum brightness in the region of the lines (in the sense that the brighter star has stronger lines) and, hence, to the luminosity ratio. We measured equivalent widths for several lines in the HV 982 spectrum and found that they indicate a ratio of  $L_S/L_P = 0.85 \pm 0.10$ , indicating that either Case 3 or Case 4 is the physically preferable solution. In an attempt to resolve this remaining degeneracy, we decided to redo the light curve analysis published by P98 using an identical computational setup (i.e., the iterative WD program). We applied the WD program to the observed light curves both individually and as a group, trying a variety of weighting schemes for the different bandpasses. The tests revealed P98's Case 4 to be a spurious solution caused by excessive weight on the Strömgren  $u$  light curve. This solution never appeared in the analysis of the well-covered  $V$  and  $I$  light curves. Therefore, our results clearly favor P98's Case 3 over the others. In Figure 3 we illustrate this solution to the  $V$  and  $I$  light curves.

The final orbital and stellar parameters adopted from the light curve analysis are listed in Table 2. These were derived from a simultaneous solution to all the bandpasses, weighted by their observational errors. Note that the longitude of the periastron  $\omega$  has been corrected to its current value (epoch 2000.0) by taking into account the apsidal motion rate  $\dot{\omega}$  from P98. The parameters  $r_P$  and  $r_S$  represent the *relative* stellar radii, i.e., the physical radii divided by the orbital semi-major axis  $a$ .

### 3.2. The Radial Velocity Curve

The radial velocity data were analyzed using the same version of the WD program as described above. In principle (i.e., with precise measurements and full phase coverage of the radial velocity curve), such an analysis can yield determinations of the component velocity semi-amplitudes  $K$  (or, equivalently, the mass ratio  $q$ ), the systemic velocity  $\gamma$ , the orbital semi-major axis  $a$ , the eccentricity  $e$ , and the longitude of the periastron  $\omega$ . In the current case, however, where dense phase coverage is impractical, it is better to adopt the well-determined values of  $e$  and  $\omega$  from the light curve solution (§3.1) and solve only for  $q$ ,  $a$ , and  $\gamma$ . This greatly simplifies the analysis since these parameters enter into the problem in a linear manner. Simulations showed that a precision of  $\sim 3\%$  in the orbital semi-major axis could be achieved with as few as eight velocity samples, as

long as phases within about  $\pm 0.1$  of the primary and secondary eclipses were excluded and a velocity precision of  $\pm 15 \text{ km s}^{-1}$  could be obtained.

Our best-fit to the radial velocity curve is shown in Figure 4. The fit residuals (indicated as “O-C” in the figure and in the last two columns of Table 1) correspond to r.m.s. errors of  $\sim 9 \text{ km s}^{-1}$ , consistent with the measurement uncertainties. Note that the details of the curve shape (such as its skewness and the abrupt changes during eclipse) are not a product of the radial velocity analysis, but rather result from the adopted light curve solution and from the physical effect of partially-eclipsed rotating stars (the “Rossiter Effect”). The unknowns in the velocity curve analysis are strictly linear scale factors and offsets — which, as noted above, is the reason that precise results can be obtained with a relatively small number of observations.

The best-fitting parameters to the radial velocity curve are listed in Table 2. It is interesting to note that the two components of the system are so similar in mass that their identity could be reversed (i.e.,  $q \equiv M_S/M_P$  is compatible with values both smaller and greater than 1). The systemic radial velocity we obtain ( $\gamma = +285 \text{ km s}^{-1}$ ) is in good agreement with general expectations for an LMC object.

### 3.3. The UV/Optical Energy Distribution

The final step in the analysis of HV 982 is modeling the observed shape of the UV/optical energy distribution. This procedure is identical to that used for HV 2274 (see Paper I), and is based on the technique developed by Fitzpatrick & Massa (1999; hereafter FM99).

For a binary system, the observed energy distribution depends on the surface fluxes of the binary's components and on the attenuating effects of distance and interstellar extinction. This relationship can be expressed as:

$$f_{\lambda \oplus} = \left( \frac{R_P}{d} \right)^2 [F_{\lambda}^P + (R_S/R_P)^2 F_{\lambda}^S] \times 10^{-0.4E(B-V)[k(\lambda-V)+R(V)]} \quad (1)$$

where  $F_{\lambda}^i \{i = P, S\}$  are the surface fluxes of the primary and secondary stars, the  $R_i$  are the absolute radii of the components, and  $d$  is the distance to the binary. The last term carries the extinction information, including  $E(B-V)$ , the normalized extinction curve  $k(\lambda-V) \equiv E(\lambda-V)/E(B-V)$ , and the ratio of selective-to-total extinction in the  $V$  band  $R(V) \equiv A(V)/E(B-V)$ .

The analysis consists of a non-linear least squares determination of the optimal values of all the parameters which contribute to the right side of equation 1. We represent the stellar surface fluxes with R.L. Kurucz's ATLAS9 atmosphere models, which each depend on four parameters: effective temperature ( $T_{\text{eff}}$ ), surface gravity, metallicity ([m/H]), and microturbulence velocity ( $\mu$ ). Thus, in principle, the problem can involve solving for two sets of Kurucz model parameters, the ratios  $(R_P/d)^2$  and  $R_S/R_P$ ,  $E(B-V)$ ,  $k(\lambda-V)$ , and  $R(V)$ . For HV 982, however, a number of simplifications can be made: (1) the temperature ratio of the two stars is known from the light curve analysis; (2) the surface gravities are known from the combined results of the light and radial velocity curve analyses; (3) the values of [m/H] and  $\mu$  can be assumed to be identical for both components; (4) the ratio  $R_S/R_P$  is known; (5) the properties of normalized UV/optical extinction are constrained by small number of parameters (Fitzpatrick & Massa 1990, Fitzpatrick 1999);

and (6) the standard mean value of  $R(V) = 3.1$  found for the Milky Way can reasonably be assumed given the existing LMC measurements (e.g., Koornneef 1982; Morgan & Nandy 1982).

With these simplifications in place, we modeled the observed UV/optical energy distribution of HV 982, solving for the best-fitting values of  $T_{\text{eff}}^P$ ,  $[\text{m}/\text{H}]_{PS}$ ,  $\mu_{PS}$ ,  $(R_P/d)^2$ ,  $E(B-V)$ , and  $k(\lambda-V)$ . Prior to the fitting procedure, the FOS data were binned to match the *ATLAS9* wavelength scale (typically 10 Å bins in the UV and 20 Å bins in the optical). These data are shown in Figure 5 (small filled circles), where the log of the observed flux is plotted against wavelength. Data points indicated by the crosses were excluded from the fit, for the reasons discussed in Paper I and FM99 (mainly due to the presence of interstellar gas absorption). We do not utilize optical photometry in this analysis, as Pritchard (private communication) notes that the transformation of these data to the standard systems is uncertain. Overplotted on the observations is our best-fitting model of HV 982's energy distribution. The value of the reduced  $\chi^2$  for the fit is close to 1 and it is clear that the model represents the data extremely well — at a level consistent with observational errors — and with no evidence for systematic deviations.

Apart from the distance and extinction attenuation, the model in Figure 5 has also been convolved with an interstellar H I Ly $\alpha$  absorption line profile corresponding to an H I column density of  $1.75 \times 10^{21} \text{ cm}^{-2}$ . This consists of an assumed Galactic foreground contribution of  $5.5 \times 10^{20} \text{ cm}^{-2}$  (see, e.g., Schwering & Israel 1991) and an LMC contribution of  $1.2 \times 10^{21} \text{ cm}^{-2}$  ( $\pm \sim 25\%$ ) determined by us from the strength of the interstellar Ly $\alpha$  absorption line in the manner of Bohlin (1975) using the original, unbinned, FOS spectrum.

The parameters derived from the energy distribution fit are listed in Table 2 along with the  $1\sigma$  internal uncertainties, which incorporate the full covariance of the parameters. Note that the derived metallicity is consistent with expectations for an LMC object. The value of  $E(B-V)$  for the system is the same, to within the errors, as that found by P98 from optical photometry. The shape of the extinction curve (which results from extinction arising in both the LMC and the Milky Way's halo) will be discussed in a forthcoming paper, combining the results for several different LMC lines of sight. We note here that it is virtually identical to that found towards HV 2274 and features a Milky Way-like UV slope, a very weak 2175 Å bump, and very weak far-UV “curvature” (using the terminology of Fitzpatrick & Massa 1990).

#### 4. THE PHYSICAL PROPERTIES OF THE HV 982 STARS

The results of the analyses described above can be combined to provide a detailed characterization of the physical properties of the HV 982 system. We summarize these properties in Table 3; notes to the Table indicate how the individual stellar properties were derived from the analysis.

It is important to realize that the results in Table 3 were derived completely independently of any stellar evolution considerations. Thus, stellar structure and evolution models can be used to provide a valuable check on the self-consistency of our empirical results. To test this consistency, we considered the evolutionary models of Claret (1995, 1997) and Claret & Giménez (1995, 1998) (altogether referred to as the CG models). These models cover a wide range in both metallicity ( $Z$ ) and initial helium abundance ( $Y$ ), incorporate the most modern input physics, and adopt a value of 0.2  $H_p$  as the convective

overshooting parameter.

The locations of the HV 982 components in the  $\log T_{\text{eff}}$  vs.  $\log L$  diagram are shown in Figure 6. The skewed rectangular boxes indicate the  $1\sigma$  error locus (recall that errors in  $T_{\text{eff}}$  and  $L$  are correlated). If our results are consistent with stellar evolution calculations, then the evolution tracks corresponding to the masses and metallicity derived from the analysis should pass through the error boxes in the  $\log T_{\text{eff}}$  vs.  $\log L$  diagram. Indeed, this is the case. The thin solid lines show the tracks corresponding to ZAMS masses of  $12.5$  and  $12.2 M_{\odot}$  and  $Z = 0.008$ . (The models predict that such stars should lose about  $0.1 M_{\odot}$  due to stellar winds by the time they reach the positions of the HV 982 stars, yielding the present-day masses of  $12.4$  and  $12.1 M_{\odot}$ .) Further, the two stars are compatible with a single isochrone, corresponding to an age of 15 Myr (dotted line in Figure 3). Note that the only adjustable parameter in the model comparison is the initial helium abundance  $Y$ , for which we find an optimal value of  $Y = 0.25 \pm 0.03$ . This value is in good agreement with expectations from empirical chemical enrichment laws (see Ribas et al. 2000b).

An additional, independent test of the compatibility of our results and stellar structure theory is possible because HV 982 has an eccentric orbit with a well-determined apsidal motion rate ( $\dot{\omega}$ ; see P98). The apsidal motion of a binary system can be computed as the sum of a general relativity term (GR) and a classical term (CL). The latter, which is the most important contribution in close systems like HV 982, depends on the internal mass distributions of the stars. A theoretical value of  $\dot{\omega}$  can be computed from the evolution models shown in Figure 3 and then compared with the observed rate.

The mass concentration parameters  $k_2$  (i.e, the ratio of the central density to mean density) for the appropriate CG models are  $\log k_{2P} = -2.33 \pm 0.03$  and  $\log k_{2S} = -2.28 \pm 0.03$ . (The error bars reflect the observational uncertainties in the stellar masses.) These values contain a small correction for stellar rotation effects, according to Claret & Giménez (1993). Using the formulae of Claret & Giménez, we compute a total theoretical apsidal motion rate of  $\dot{\omega}(\text{th}) = 2.05 \pm 0.32 \text{ deg/yr}$ , in which  $\dot{\omega}_{\text{CL}} = 1.94 \text{ deg/yr}$  is the classical term and  $\dot{\omega}_{\text{GR}} = 0.11 \text{ deg/yr}$  is the general relativistic contribution. This theoretical estimate agrees with the observed value of  $\dot{\omega}(\text{obs}) = 1.76 \pm 0.06 \text{ deg/yr}$  to within the expected uncertainties, again indicating consistency between our empirical results and stellar interiors theory. It is interesting to note that this agreement, although satisfactory, would be enhanced by increasing the convective overshooting parameter in the CG models, as suggested by the results of Guinan et al. (2000) and Ribas, Jordi, & Giménez (2000).

#### 5. THE DISTANCE TO HV 982 AND THE LMC

Our analysis has yielded a picture of HV 982 as consisting of a pair of normal, mildly-evolved, early-B stars. The results are all internally consistent and consistent with a host of external “reality checks,” such as the expected LMC metallicity,  $M_V$  calibrations of Galactic B stars, and stellar evolution calculations. This detailed characterization and the unremarkable nature of HV 982 make this system ideal for the determination of a precise distance.

As in Paper I, we derive the distance simply by combining results from the EB analysis — which yield the absolute radius of the primary star  $R_P$  — and from the spectrophotometry analysis — which yields the distance attenuation factor  $(R_P/d)^2$ . The result, shown in Table 3, is  $d_{\text{HV982}} = 45.6 \pm 2.1 \text{ kpc}$ , corresponding to a distance modulus of  $(V_0 - M_V)_{\text{HV982}} = 18.29 \pm 0.10$ . The

uncertainty in these values arises from 3 independent sources: (1) the internal measurement errors in  $R_A$  and  $(R_A/d)^2$  (see Table 2); (2) uncertainty in the appropriate value of the extinction parameter  $R(V)$ ; and (3) uncertainty in the FOS flux scale. These three factors yield individual uncertainties of  $\pm 1.7$  kpc,  $\pm 1.1$  kpc (assuming  $\sigma R(V) = \pm 0.3$ ), and  $\pm 0.6$  kpc (assuming  $\sigma f(FOS) = \pm 2.5\%$ ), respectively. The overall  $1\sigma$  uncertainty quoted above is the quadratic sum of these three errors.

Note that the distance to HV 982 can also be derived by computing a distance modulus directly from the values of  $M_V$  listed in Table 3 and an extinction-corrected  $V$  magnitude. However, while this yields essentially the same result as above, it is subject to the uncertainties in the optical photometry and in the bolometric corrections used to compute the absolute magnitudes.

To estimate the mean distance to the LMC from the HV 982 results, we adopt as a reference point the optical center of the LMC's bar, at  $(\alpha, \delta) = (5^h 24^m, -69^\circ 47')$  according to Isserstedt (1975), and assume a disk inclination of  $38^\circ$  and a line-of-nodes position angle of  $168^\circ$  (Schmidt-Kaler & Gohermann 1992). Figure 7 shows a photo of the LMC with the adopted center and the orientation of the line-of-nodes indicated by the open box and solid line, respectively. The “nearside” of the LMC is eastward of the line-of-nodes. The HV 982 system is located relatively close to the line-of-nodes, as shown in the figure, and simple trigonometry indicates that it lies about 300 pc in front of the bar center. Our analysis of HV 982 thus yields  $d_{LMC} = 45.9 \pm 2.1$  kpc, corresponding to  $(V_0 - M_V)_{LMC} = 18.31 \pm 0.10$ .

This result is entirely consistent with our earlier analysis of the system HV 2274 (Paper I) which yielded  $d_{LMC} = 45.7 \pm 1.6$  kpc, corresponding to  $(V_0 - M_V)_{LMC} = 18.30 \pm 0.07$ . The very close agreement is probably a fluke of small number statistics, but could also indicate that the error analysis is somewhat conservative. Only further measurements of other systems can address this. Note that the actual distance derived for HV 2274 itself, 46.8 kpc, is greater by 1.2 kpc than that of HV 982, and consistent with its apparent position on the “farside” of the LMC's line-of-nodes (see Figure 7). The close agreement in the implied distances to the LMC bar center is thus partly dependent on the assumed inclination and position angles of the LMC, although changes in these values (within their observed ranges) affect the agreement by only a few hundred pc.

The HV 2274 distance from Paper I has been challenged by Udalski et al. (1998) and Nelson et al. (2000) who advocate (small) adjustments in opposite directions. Neither of these adjustments is warranted, however. We believe it is not reasonable to assume, as Udalski et al. do, that the interstellar reddening towards HV 2274 can be derived more precisely from stars of unknown spectral type in its field — whose spatial distribution relative to HV 2274 is unknown — than from detailed analysis of HV 2274 itself. It is encouraging, however, that the two different methods yield very similar results. Nelson et al. advocate a significantly smaller reddening than found in Paper I, based on their new *UBV* photometry of the system. Our FOS spectrophotometry of HV 2274 is simply not consistent with their results and it seems likely that errors in the transformation of Nelson et al.'s photometry to the standard system are larger than they estimate. Table 2 of Nelson et al. illustrates the significant discrepancies that exist among various photometric measurements of HV 2274. Our results are consistent with the *UBV* data reported by Udalski et al.

The transformation of the HV 982 and HV 2274 distances to a general LMC distance implicitly assumes that the two bi-

nary systems are associated with the main mass of the LMC and do not occupy peculiar positions — most particularly that they do not lie significantly in front of the the Cloud. While this seems plausible on general principles, it can also be shown to be true specifically by considering the interstellar absorption present in the spectra of the two systems. In §3.3 we derived a column density of  $N(\text{H I}) = 1.2 \times 10^{21} \text{ cm}^{-2}$  for LMC H I gas located *in front of* HV 982 from the H I Ly $\alpha$  absorption line in the FOS data. A similar analysis of the HV 2274 data yields a LMC column density of  $N(\text{H I}) = 6.0 \times 10^{20} \text{ cm}^{-2}$ . In both cases the uncertainties are of order 25%. From the H I 21-cm emission line data of Rohlfs et al. (1984) we see that the *total* LMC H I column densities along the HV 982 and HV 2274 lines of sight are about  $9.0 \times 10^{20} \text{ cm}^{-2}$  and  $1.0 \times 10^{21} \text{ cm}^{-2}$ , respectively. HV 2274 is clearly embedded in the main H I mass along its line of sight, while HV 982 is located behind most of H I gas along its direction. The reddenings derived for the two systems also indicate that they cannot be sitting out in front of the rest of the LMC, since the systems are considerably more reddened than can be accounted for by Galactic foreground material (Oestreicher, Gohermann, & Schmidt-Kaler 1995). It is thus reasonable to assume that the distances of HV 982 and HV 2274 are representative of the main body of the LMC.

## 6. CONCLUSIONS

The complete analyses of two LMC EB systems, HV 2274 (Paper I) and HV 982 (this paper) have yielded two consistent measurements of the distance to the center of the LMC. Formally combining the two results yields  $d_{LMC} = 45.8 \pm 1.5$  kpc. The overall uncertainty is not much reduced from that originally quoted in Paper I for HV 2274 because only the internal errors due to  $\sigma R_A$  and  $\sigma(R_A/d)^2$  are independent of each other. The errors associated with the FOS flux scale and the uncertainty in  $R(V)$  are systematic and do not diminish by combining these two results. The internal error in the HV 982 and HV 2274 analyses could each be improved by additional observations, particularly, better sampling of the radial velocity curves and extended spectrophotometric wavelength coverage. Observations in the near-IR could also help reduce the uncertainty in the appropriate value of  $R(V)$ . (We assumed above that the uncertainty in  $R(V)$  is common to both HV 982 and HV 2274, and not reduced by combining results, because the shapes of the optical/UV portions of their extinction curves are very similar, suggesting equally similar  $R(V)$  values.)

These results argue strongly in favor of the “short” LMC distance scale. For the “long” scale to be tenable (i.e.,  $d \simeq 55$  kpc), the HV 982 and HV 2274 systems would have to lie about 10 kpc in front of the main body of the LMC, which we have shown to be inconsistent with the interstellar absorption data.

Despite the level of uncertainty still present, it is worth exploring briefly the implication of the current results. The cosmological importance of the LMC distance is that it serves as the meter stick by which the Cepheid variable distance scale is currently calibrated. This significance is nicely illustrated by Mould et al.'s (2000) characterization of current best value for  $H_0$  in terms of the LMC distance, i.e.,  $H_0 = 3.5 \pm 0.2 \text{ km s}^{-1}$  per LMC distance. The value of  $d_{LMC} = 46$  kpc found here then indicates  $H_0 \simeq 76 \text{ km s}^{-1} \text{ Mpc}^{-1}$ . In more graphic terms, this result implies a shrinkage of about 8% in the linear scale of the Universe, as compared to the *HST* Key Project result (which is based on an assumed LMC distance of 50 kpc). Such a change has numerous ramifications, but of particular interest is that the current result reconciles the discrepancy between the Cepheid-

based distance to the galaxy NGC 4258 ( $8.1 \pm 0.4$  Mpc; Maoz et al. 1999) and a very secure distance based on the orbital motion of water masers around the supermassive black hole at its center ( $7.2 \pm 0.2$  Mpc; Herrnstein et al. 1999).

While further observations could help sharpen the HV 2274 and HV 982 results, it is clear that analysis of additional EB systems will do the most to demonstrate the reliability of this method. During December 2000 we will observe several detached EBs with the 4-m Blanco telescope at CTIO to obtain radial velocity curves. In addition, we were awarded 32 orbits with the *Hubble Space Telescope* during Cycle 9 to carry out spectrophotometric and radial velocity studies of three additional systems well-suited for distance determinations. The locations of these objects (EROS 1044, EROS 1066, MACHO 053648.7-691700) are shown in Figure 7. All lie within or near to the LMC bar and the MACHO EB was selected to be close to the position (within 7 arcmin) of SN 1987A in the 30 Dor complex. This will provide a cross-check between the two most direct methods for determining the distance to the LMC.

Analysis of 8-10 well-suited EBs potentially can result in

a LMC distance measurement with a net uncertainty of  $(V_0 - M_V)_{\text{LMC}} \simeq 0.03$  mag (< 1.5%). Within the next few years we hope to expand the program to include about 20 systems. Recent n-body simulations of the tidal interaction of the Milky Way with the LMC indicate that its structure may be more extended and complex than presently assumed (see Weinberg 2000). The ensemble of targets, in addition to nailing down the distance to the LMC, will provide a detailed probe of the structure and spatial extent of this important galaxy.

This work was supported by NASA grants NAG5-7113 and HST GO-06683, and NSF/RUI AST-9315365. We are grateful for the skilled assistance of the CTIO support staff during our January 2000 observing run. E.F. acknowledges support from NASA ADP grant NAG5-7117 to Villanova University and thanks Michael Oestreich for kindly making his LMC foreground extinction data available. I.R. acknowledges the Catalan Regional Government (CIRIT) for financial support through a postdoctoral Fulbright fellowship.

#### REFERENCES

Andersen, J. 1975, A&A, 44, 355  
 Bohlin, R. 1975, ApJ, 200, 402  
 Claret, A. 1995, A&AS, 109, 441  
 Claret, A. 1997, A&AS, 125, 439  
 Claret, A., & Giménez, A. 1993, A&A, 277, 487  
 Claret, A., & Giménez, A. 1995, A&AS, 114, 549  
 Claret, A., & Giménez, A. 1998, A&AS, 133, 12  
 Cole, A.A. 1998, ApJ, 500, L137  
 Fitzpatrick, E.L. 1999, PASP, 111, 63  
 Fitzpatrick, E.L., & Massa, D. 1990, ApJS, 72, 163  
 Fitzpatrick, E.L., & Massa, D. 1999, ApJ, 525, 1011 (FM99)  
 Flower, P.J. 1996, ApJ, 469, 355  
 Guinan, E.F., Fitzpatrick, E.L., DeWarf, L.E., Maloney, F.P., Maurone, P.A., Ribas, I., Pritchard, J.D., Bradstreet, D.H., & Giménez, A. 1998, ApJ, 509, L21 (Paper I)  
 Guinan, E.F., Ribas, I., Fitzpatrick E.L., Giménez A., Jordi C., McCook G.P., & Popper D.M. 2000, ApJ, in press (astro-ph/0005029)  
 Herrnstein, J. R., Moran, J. M., Greenhill, L. J., Diamond, P. J., Inoue, M., Nakai, N., Miyoshi, M., Henkel, C., & Riess, A. 1999, Nature, 400, 539  
 Isserstedt, J. 1975, A&A, 41, 21  
 Koornneef, J. 1982, A&A, 107, 247  
 Maoz, E., Newman, J.A., Ferrarese, L., Stetson, P.B., Zepf, S.E., Davis, M., Freedman, W.L., & Madore, B.F. 1999, Nature, 401, 351  
 Milone, E.F., Stagg, C.R., & Kurucz, R.L. 1992, ApJS, 79, 123  
 Morgan, D.H., & Nandy, K. 1982, MNRAS, 199, 979  
 Mould, J.R., et al. 2000, ApJ, 529, 786  
 Nelson, C.A., Cook, K.H., Popowski, P., & Alves, D.R. 2000, AJ, 119, 1205  
 Oestreich, M.O., Gochermann, J., & Schmidt-Kaler, T. 1995, A&AS, 112, 495  
 Pritchard, J.D., Tobin, W., Clark, M., & Guinan, E.F. 1998, MNRAS, 299, 1087 (P98)  
 Ribas, I., Jordi, C., & Giménez, A. 2000, MNRAS, in press  
 Ribas, I., Jordi, C., Torra, J., & Giménez, A. 2000b, MNRAS, 313, 99  
 Ribas, I., Guinan, E.F., Fitzpatrick, E.L., DeWarf, L.E., Maloney, F.P., Maurone, P.A., Bradstreet, D.H., Giménez, A., & Pritchard, J.D. 2000a, ApJ, 528, 692  
 Rohlfs, K., Kreitschmann, J., Siegman, B.C., & Feitzinger, J.V. 1984, A&A, 137, 343  
 Schmidt-Kaler, T., & Gochermann, J. 1992, in "Variable Stars and Galaxies", ed. B. Warner, A.S.P. Conf. Series, vol. 30, p. 203  
 Schwerling, P.B.W., & Israel, F.P. 1991, A&A, 246, 231  
 Udalski, A., Pietrzynski, G., Wozniak, P., Szymanski, M., Kubiak, M., & Zebrun, K. 1998, ApJ, 509, L25  
 Westerlund, B.E. 1997, *The Magellanic Clouds*, (Cambridge University Press, Cambridge)  
 Weinberg, M.D. 2000, ApJ, 532, 922  
 Wilson, R.E., & Devinney, E.J. 1971, ApJ, 166, 605 (WD)

TABLE 1  
HELIOCENTRIC RADIAL VELOCITY MEASUREMENTS FOR HV 982

HJD (-2451500)	Orbital Phase	RV <sub>P</sub> (km s <sup>-1</sup> )	RV <sub>S</sub> (km s <sup>-1</sup> )	(O-C) <sub>P</sub> (km s <sup>-1</sup> )	(O-C) <sub>S</sub> (km s <sup>-1</sup> )
58.6813	0.7203	440 ± 10	128 ± 9	-0.9	3.0
58.7073	0.7252	435 ± 9	123 ± 10	-3.6	-3.0
60.6335	0.0886	187 ± 16	386 ± 31	-3.6	4.4
60.7966	0.1168	174 ± 10	421 ± 12	7.6	14.6
61.7346	0.2926	95 ± 10	463 ± 8	-4.1	-11.7
61.7569	0.2968	95 ± 12	464 ± 11	-5.8	-9.8
61.7823	0.3016	114 ± 10	482 ± 13	10.8	11.5
63.7490	0.6702	459 ± 15	110 ± 12	14.0	-10.1

TABLE 2  
RESULTS FROM LIGHT CURVE, RADIAL VELOCITY CURVE, AND SPECTROPHOTOMETRY ANALYSES

Parameter	Value
<i>Light Curve Analysis</i>	
Period (days)	5.335220 ± 0.000003
Eccentricity	0.161 ± 0.005
Inclination (deg)	89.8 ± 1.5
$\omega$ (2000.0) (deg)	236.2 ± 0.5
$\dot{\omega}$ (deg/yr) <sup>a</sup>	1.76 ± 0.06
$\frac{T_{\text{eff}}^S}{T_{\text{eff}}^P}$	0.984 ± 0.005
$\frac{L_S}{L_P} \Big _{V,I}$	0.81 ± 0.02
$r_P \equiv \frac{R_P}{a}$	0.215 ± 0.002
$r_S \equiv \frac{R_S}{a}$	0.197 ± 0.002
<i>Radial Velocity Curve Analysis</i>	
$K_P$ (km s <sup>-1</sup> )	176.9 ± 6.5
$K_S$ (km s <sup>-1</sup> )	181.6 ± 6.5
$q \equiv \frac{M_S}{M_P}$	0.974 ± 0.050
$\gamma$ (km s <sup>-1</sup> )	284.5 ± 4.2
$a$ (R <sub>⊕</sub> )	37.3 ± 1.0
<i>Energy Distribution Analysis</i>	
$T_{\text{eff}}^P$ (K)	25050 ± 300
[m/H] <sub>PS</sub>	-0.48 ± 0.06
$\mu_{PS}$ (km s <sup>-1</sup> )	0
E(B-V) (mag)	0.169 ± 0.014
$(R_P/d)^2$	1.570 ± 0.080 × 10 <sup>-23</sup>

<sup>a</sup>From P98

TABLE 3  
PROPERTIES OF THE HV 982 SYSTEM

Property	Primary Star	Secondary Star
Spectral Type <sup>a</sup>	B1 V-IV	B1 V-IV
Mass ( $M_{\odot}$ ) <sup>b</sup>	$12.4 \pm 0.7$	$12.1 \pm 0.7$
Radius ( $R_{\odot}$ ) <sup>c</sup>	$8.02 \pm 0.23$	$7.35 \pm 0.21$
$\log g$ (cgs) <sup>d</sup>	$3.723 \pm 0.035$	$3.788 \pm 0.035$
$T_{eff}$ (K) <sup>e</sup>	$25050 \pm 300$	$24700 \pm 300$
$\log(L/L_{\odot})$ <sup>f</sup>	$4.36 \pm 0.03$	$4.26 \pm 0.03$
[Fe/H] <sup>g</sup>	$-0.36 \pm 0.06$	$-0.36 \pm 0.06$
$M_{bol}$ (mag) <sup>h</sup>	$-6.15 \pm 0.08$	$-5.90 \pm 0.08$
$M_V$ (mag) <sup>i</sup>	$-3.7$	$-3.5$
$d_{HV982}$ (kpc) <sup>j</sup>		$45.6 \pm 2.1$
$d_{LMC}$ (kpc) <sup>k</sup>		$45.9 \pm 2.1$

<sup>a</sup>Estimated from  $T_{eff}$  and  $\log g$

<sup>b</sup>From the mass ratio  $q$  and the application of Kepler's Third Law.

<sup>c</sup>Computed from the relative radii  $r_P$  and  $r_S$  and the orbital semimajor axis  $a$ .

<sup>d</sup>Computed from  $g = GM/R^2$

<sup>e</sup>Direct result of the spectrophotometry analysis.

<sup>f</sup>Computed from  $L = 4\pi R^2 \sigma T_{eff}^4$

<sup>g</sup>Direct result of the spectrophotometry analysis, adjusted by +0.12 dex to account for the overabundance of Fe in the Kurucz ATLAS9 opacities. See FM99.

<sup>h</sup>Computed from  $\log(L/L_{\odot})$  and  $M_{bol\odot} = 4.75$

<sup>i</sup>Computed from  $M_{bol}$  and a bolometric correction of  $BC = -2.41$  taken from Flower 1996 for  $T = 25000$  K. Note that this result is consistent with expectations for mildly evolved early-B stars.

<sup>j</sup>Using  $(R_P/d)^2$  from the spectrophotometry analysis and  $R_P$  from the light/radial velocity curve analysis

<sup>k</sup>Distance to the center of the LMC, derived from  $d_{HV982}$  as described in §5.

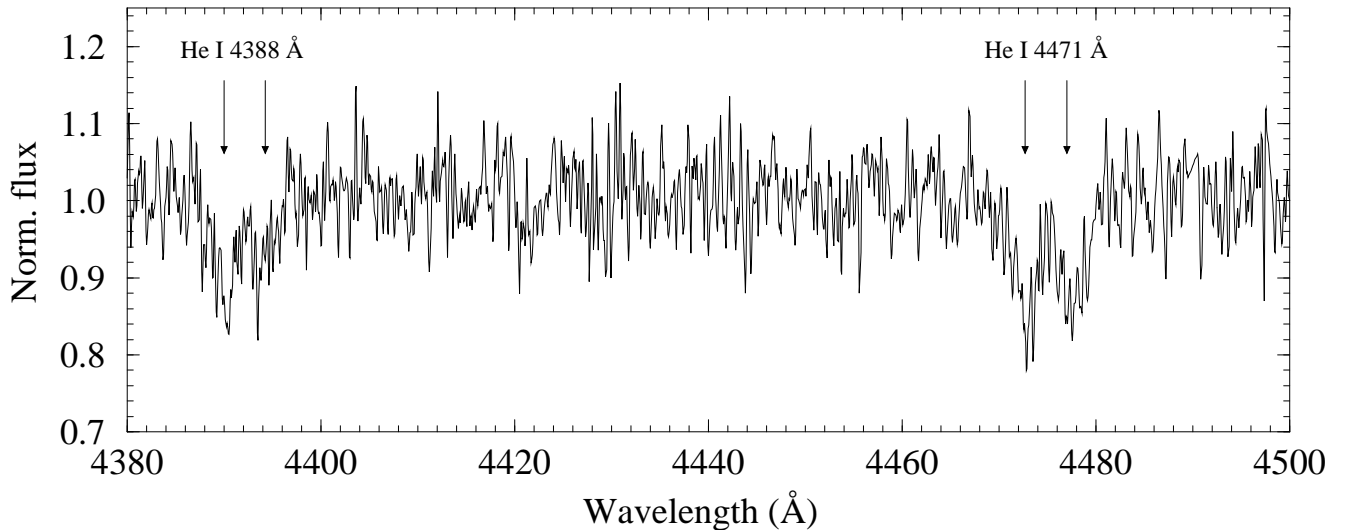


FIG. 1.— Normalized spectrum of HV 982 near the prominent He I 4388 and 4471 Å lines. The spectrum was obtained with the Blanco 4-m telescope at Cerro Tololo Inter-American Observatory on HJD 2451558.7073 at binary phase 0.7252. The velocity separation between the primary and secondary stars at this phase is  $\Delta v = 312 \text{ km s}^{-1}$ . This figure demonstrates that the absorption lines from the two stars are cleanly resolved and, thus, that the radial velocity measurements will be immune to blending effects.

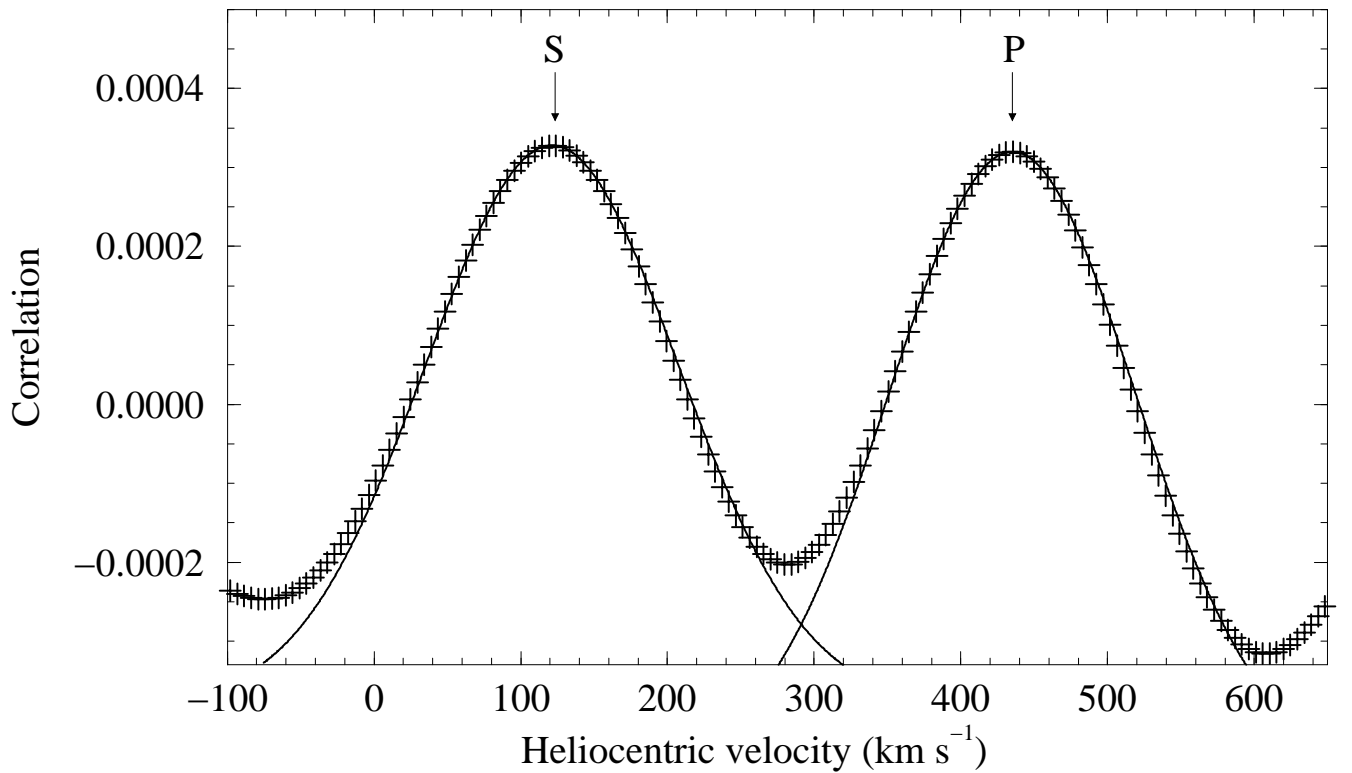


FIG. 2.— Cross correlation between the HV 982 spectrum obtained on HJD 2451558.7073 and the velocity template star HR 1443 (plus signs). The cross correlation was performed with the IRAF procedure FXCOR using data in the range 4000–5000 Å. The H  $\beta$ , H  $\gamma$  and H  $\delta$  lines were masked by setting the normalized flux to unity in a window around their central wavelengths. The spectra were filtered in FXCOR prior to the cross correlation, using a Fourier ramp filter to remove both high and low frequencies. The filter was tuned using cross correlations among several observed velocity template stars. The velocity peaks of the primary ("P") and secondary ("S") stars are fully resolved and the actual velocities were determined by fitting Gaussians to the peaks (solid curves). The velocity peaks shown in the figure are 4–5 times higher than the r.m.s. noise in the cross correlation function.

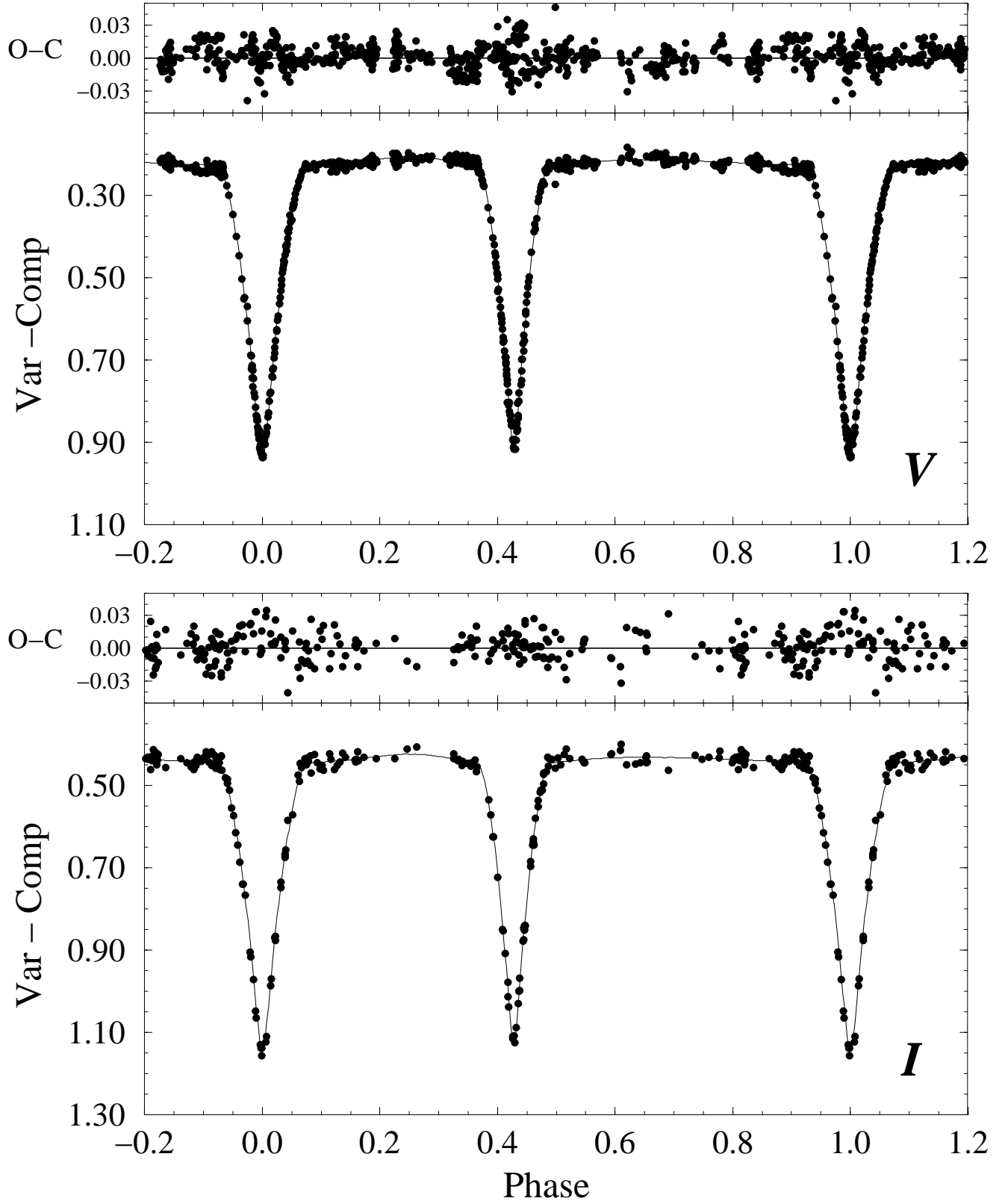


FIG. 3.—  $V$  and  $I$  light curves for HV 982 (filled circles) overplotted with the best fitting model (solid curves). The residuals to the fits (“O-C”) are shown above each light curve. The parameters derived from the fit are listed in Table 2. The data are from P98 and the final solution is identical to P98’s Case 3.

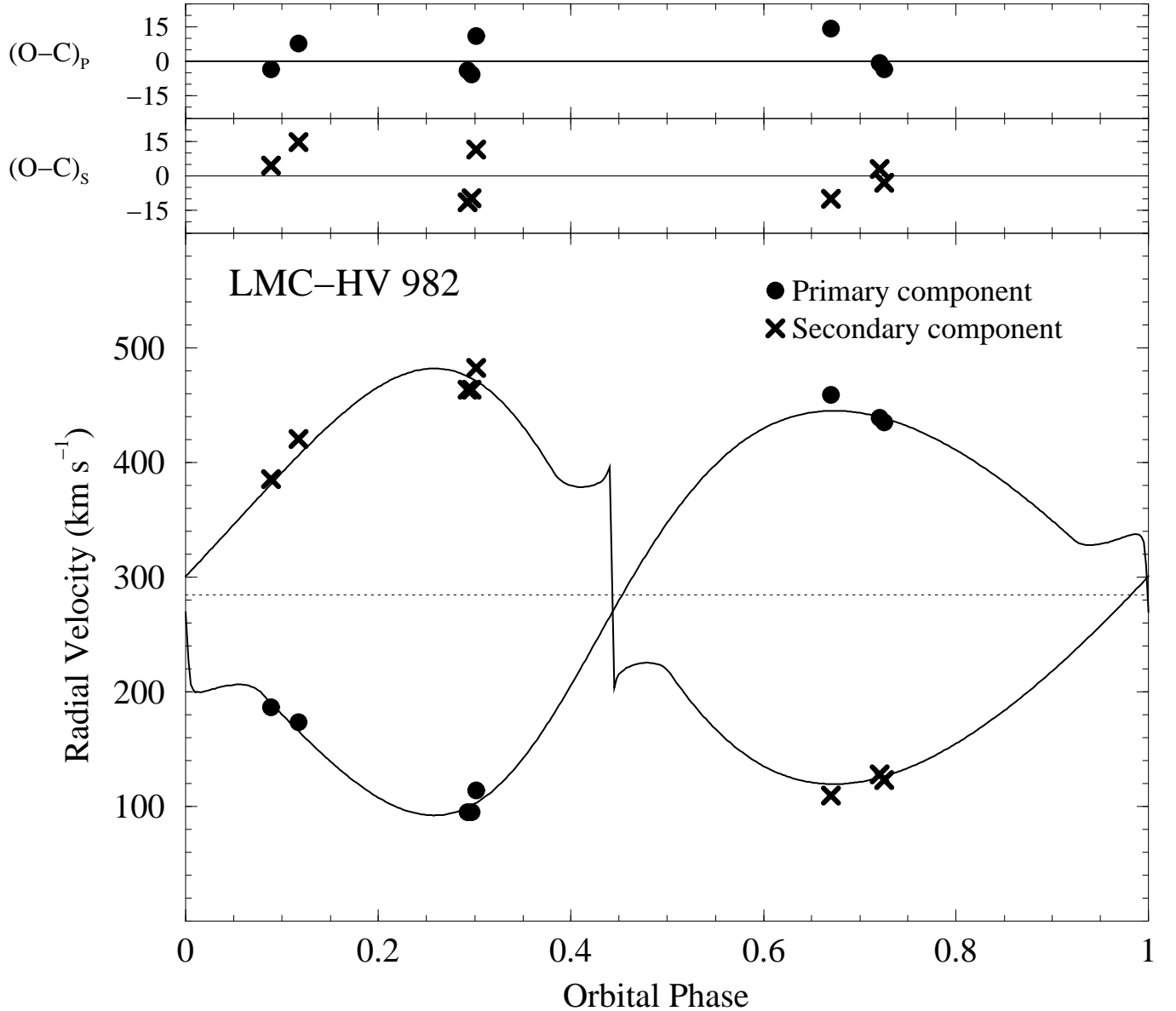


FIG. 4.— Radial velocity data for HV 982 (see Table 1) superimposed with best-fitting model. The parameters derived from the data are listed in Table 2. Note that the details of the model curve, including the sharp discontinuity due to the partial eclipse of a rotating star (the Rossiter Effect), are not a product of the radial velocity curve analysis. The fit assumed the values of the orbital eccentricity, inclination, and longitude of periastron found from the light curve. The parameters directly determined from the radial velocity curve, i.e., the velocity semi-amplitudes  $K$  and the systemic velocity  $\gamma$ , enter into the problem as linear offsets or scale factors. The residuals to the fit are shown above the radial velocity curve and indicate r.m.s. uncertainties in the data of  $\sim 9$   $\text{km s}^{-1}$  for both the primary and secondary components.

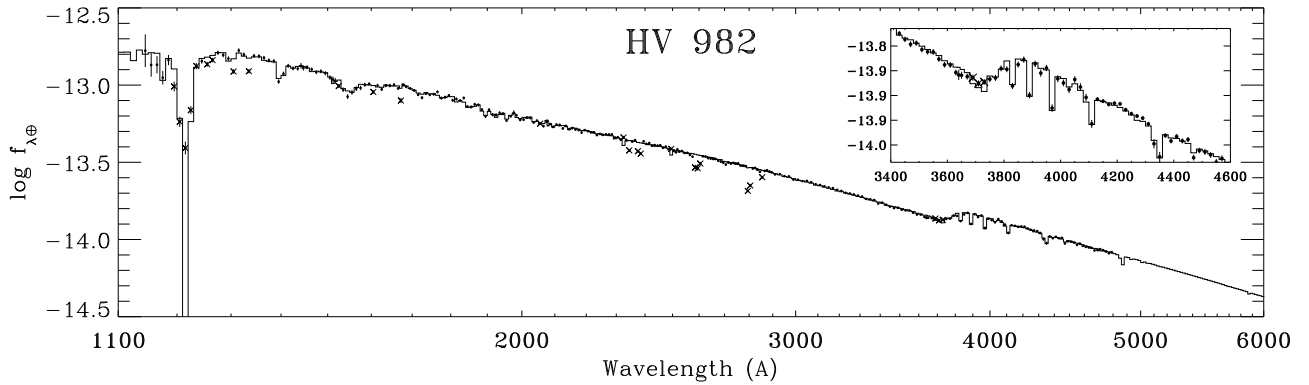


FIG. 5.— The observed UV/optical energy distribution of the HV 982 system (small filled circles) in units of  $\text{ergs cm}^{-2} \text{ s}^{-1} \text{ \AA}^{-1}$ , superimposed with the best-fitting model, consisting of a pair of reddened and distance-attenuated Kurucz ATLAS9 atmosphere models (histogram-style line). Vertical lines through the data points indicate the  $1\sigma$  observational errors. Crosses denote data points excluded from the fit, primarily due to contamination by interstellar absorption lines. The inset shows a blowup of the region surrounding the Balmer Jump. The parameters derived from the fit to the energy distribution are listed in Table 2. The various constraints imposed on the fit are discussed in §3.3.

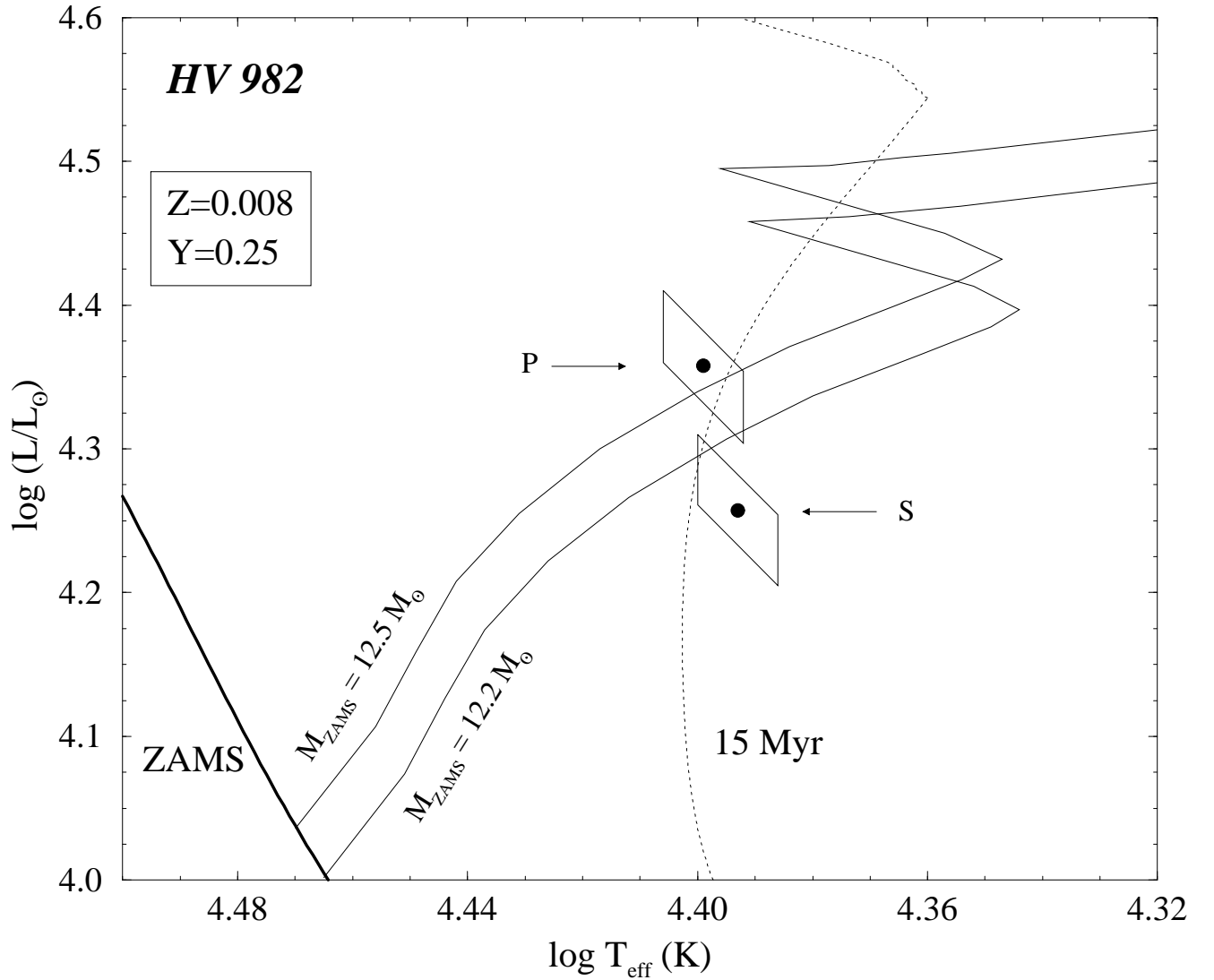


FIG. 6.— A comparison of the HV 982 results with stellar evolution theory. The positions of the the primary (P) and secondary (S) components of HV 982 on the  $\log L$  vs.  $\log T_{\text{eff}}$  diagram are indicated by the filled circles. The skewed rectangles represent the  $1\sigma$  error boxes. The position of the Zero Age Main Sequence (ZAMS) is noted. The two stellar evolution tracks shown (solid curves) are not “best fits.” They correspond to the masses derived from the binary analysis (which are  $\sim 0.1 M_{\odot}$  smaller than the original ZAMS masses due to stellar wind mass loss) and the metallicity measured from the UV/optical spectrophotometry. Only the helium abundance Y has been adjusted and the resultant value lies well within the expected range. The dotted line shows an isocrone corresponding to an age of 15 million years. The source and properties of the evolution tracks are discussed in §4.

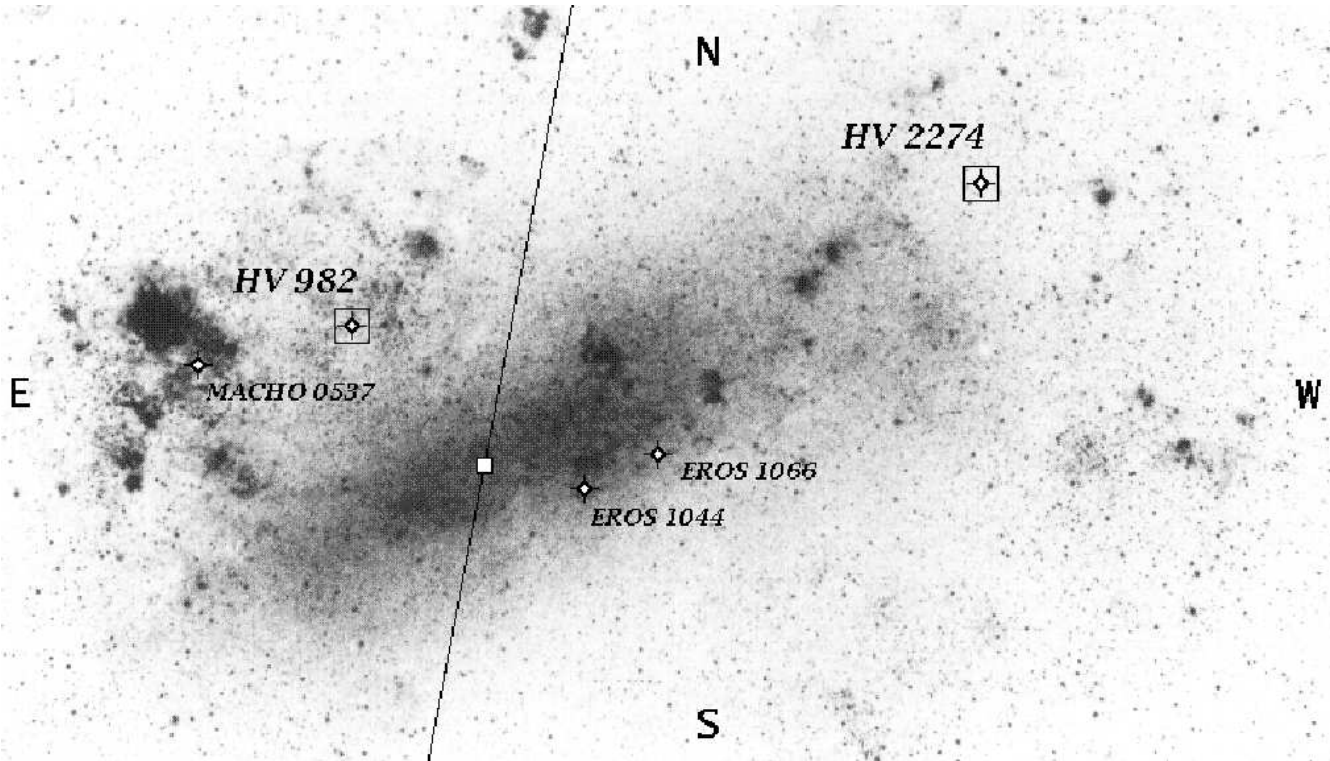


FIG. 7.—A photo of the Large Magellanic Cloud indicating the locations of HV 982 (this paper), HV 2274 (Paper I), and three targets of future observations, EROS 1044, EROS 1066, and MACHO 053648.7-691700 (labeled in the figure as MACHO 0537). The optical center of the LMC's bar according to Isserstedt 1975 is indicated by the open box and the LMC's line of nodes, according to Schmidt-Kaler & Goehermann 1992, is shown by the solid line. The “nearside” of the LMC is to the east of the line of nodes. Photo reproduced by permission of the Carnegie Institution of Washington.